Cerium doped dendritic mesoporous bioactive glass nanoparticles with bioactivity and drug delivery capability

Zhiyan Xu[1], Emily Keller[1], Ana M. Beltrán[3], Kai Zheng[2*], Aldo R. Boccaccini[1*]

[1]Institute of Biomaterials, University of Erlangen-Nuremberg, Erlangen 91058, Germany

[2]Jiangsu Province Engineering Research Center of Stomatological Translational Medicine & Jiangsu Key Laboratory of Oral Diseases, Nanjing Medical University, Nanjing 210029, China

[3]Departamento de Ingeniería y Ciencia de los Materiales y del Transporte, Escuela Politécnica Superior, Universidad de Sevilla, Virgen de África 7, Sevilla 41011, Spain

[*]Corresponding authors

E-mail address: kaizheng@njmu.edu.cn (Kai Zheng), aldo.boccaccini@fau.de (Aldo R. Boccaccini)

Abstract

Dendritic mesoporous bioactive glass nanoparticles (DMBGNs) with unique three-dimensional structures are attracting increasing attention for biomedical applications. However, it is still challenging to tune the chemical composition of DMBGNs. In this work, we provide for the first time a feasible post-impregnation approach to incorporate metallic ions (Ca and Ce) into dendritic mesoporous silica nanoparticles, resulting in SiO_2-CaO (DMBGNs) and SiO_2-CaO-CeO_2 (Ce-DMBGNs) without destroying the dendritic mesoporous topography. Both DMBGNs and Ce-DMBGNs were amorphous, negatively charged, with a hydrodynamic size of ~200 nm. The synthesized DMBGNs and Ce-DMBGNs exhibited high bioactivity as evidenced by the rapid formation of hydroxyapatite (HA) after immersion in simulated body fluid (SBF) for 7 days. In addition, DMBGNs and Ce-DMBGNs showed high propolis loading efficiency and sustained release behavior. The results suggest that developed Ce-DMBGNs have the potential to be used as a delivery vehicle of therapeutic ions and drugs in bone regeneration applications.

Keywords: Cerium; Bioactive glass; Dendritic mesoporous nanoparticle; Bioactivity; Drug delivery

1. Introduction

Mesoporous bioactive glass nanoparticles (MBGNs) are gaining tremendous attention in a variety of biomedical applications, from tissue engineering to drug delivery as a result of their remarkable properties [1]–[3]. Compared to conventional bioactive glasses (BGs), MBGNs produced by sol-gel approaches possess controllable morphologies with large specific surface area, uniform pore distribution, and ordered pore channels [3]–[5]. In particular, dendritic mesoporous silicate bioactive glass nanoparticles (DMBGNs) with hierarchically porous structures and open 3D center-radial channels are becoming promising platforms in the area of biomedicine for delivering therapeutic biomolecules and inorganic ions [6]–[8]. However, it is still challenging to incorporate therapeutic ions (particularly metallic ions) into DMBGNs due to the usually reported complicated synthesis processes of these nanoparticles [9]. In conventional synthesis of dendritic mesoporous silicate nanoparticles, multiple organic solvents and templates are usually required. The required precursors (usually salts) may interact with these organic species, resulting in distorted mesoporous structures [10]. In addition, the required washing steps for removing excessive organic solvents and templates prevent the incorporation of metallic ions into nanoparticles [11]. In our previous study, we applied organic solvent-free synthesis to obtain SiO_2-CaO DMBGNs [7]. A post impregnation approach was applied to include Ca ions, avoiding the deformation of the well-formed dendritic mesopores [7]. This post impregnation strategy is expected to be able to introduce other metallic ions into DMBGNs.

Incorporation of therapeutic agents or/and biologically active ions is a convenient approach to endow BGs with multifunctional properties including antioxidant, anti-inflammatory, angiogenesis, and antibacterial effects [12], [13]. It is worth noting that cerium (Ce), a rare-earth element with antioxidant activities, has potential as catalase and superoxide dismutase to limit the reactive oxygen species level in the body, which can be attributed to the switching in oxidation states between Ce^{3+} and Ce^{4+} in physiological fluids [14]–[16]. Ce doped BGs have been evidenced to present antioxidant, antibacterial, osteogenic and angiogenic properties [16], [17]. However, incorporation of Ce into multifunctional DMBGNs has not been reported yet. Given the unique pore structure and desirable composition, Ce-doped DMBGNs (Ce-DMBGNs) are promising materials for the delivery of therapeutic ions and biomolecules.

Herein, SiO_2-CaO-CeO_2 (Ce-DMBGNs) were firstly synthesized by using a dual-templating strategy in a facile and green synthesis route followed by post impregnation of ions (Ca and Ce). Ca and Ce ions were included into DMSNs separately. The morphology, composition, structure, and bioactivity of the synthesized nanoparticles were investigated.

In order to evaluate the drug delivery capability of Ce-DMBGNs, we also investigated the drug loading and release behavior of the nanoparticles using propolis as the target drug. Propolis is a naturally non-toxic resinous mixture produced by honeybee, exhibiting a wide range of biological activities such as antibacterial, antiviral, antifungal, antioxidant, and anti-inflammatory properties [18], [19]. This resinous mixture (more than 300 constituents depending on the source) is composed of 50 % resin, 30 % wax,

10 % essential oils, 5 % pollen and 5 % other organic compounds, of which polyphenols are regarded as the main pharmaceutically effective molecules [20]. On account of its therapeutic advantages and cost-effective feature, propolis is considered attractive in medical care, e.g., oral and dermatological applications [19]. The combination of BGs and polyphenols has been shown to exhibit synergistic effects leading to improved therapeutic outcomes [21]. Therefore, we used propolis for this drug delivery study considering the potential of Ce-DMBGNs/propolis formulations for biomedical applications.

2. Materials and methods

2.1. Synthesis of DMBGNs and Ce-DMBGNs

To synthesize DMBGNs, a two-step process was performed as reported in the previous study with slight modification [7]. Firstly, dendritic mesoporous silica nanoparticles (DMSNs) were produced using a sol-gel approach in a dual-template and organic solvent-free reaction system. Briefly, 1.52 g of cetyltrimethylammonium bromide (CTAB), 0.38 g of sodium dodecyl benzene sulfonate (SDBS), and 0.34 g of triethanolamine (TEA) were dissolved in 100 mL of deionized (DI) water under stirring at 80 ◦C for 1 h. 15.51 mL of tetraethyl orthosilicate (TEOS) were added afterwards and stirred continuously for another 2 h. The obtained nanoparticles were collected and washed by centrifuge, and then dried at 60 ◦C overnight. In regard to the incorporation of Ca, 0.15 g of produced silica nanoparticles were dispersed in 20 mL of 0.25 M calcium nitrate aqueous solution (molar ratio of Ca/Si = 2) at 25 ◦C. After

stirring for 1 h, the modified nanoparticles were collected and dried overnight. To incorporate Ce, the dried nanoparticles were redispersed in ethanol solution of cerium nitrate (0.01 M, 0.03 M and 0.05 M, respectively) at 16 mg/mL and stirred for 30 min at 25 ◦C. The obtained Ce-DMBGNs were labelled as 1Ce-DMBGNs, 3Ce-DMBGNs and 5Ce-DMBGNs, respectively. After the impregnation process, the resulting nanoparticles were washed three times with ethanol and dried overnight in an electric oven at 60 ◦C.

All dried nanoparticles were eventually calcinated at 700 ◦C for 5h 30 min with a heating rate of 2 ◦C/min. All used chemicals were purchased from Sigma-Aldrich (Darmstadt, Germany) and used as received without further purification.

2.2. Characterization

The morphology of nanoparticles was observed using field-emission scanning electron microscopy (FE-SEM, Auriga, Carl Zeiss, Germany) and scanning-transmission electron microscopy (S-TEM, FEI Talos F200S, Thermo Fischer Scientific, US). Energy dispersive X-ray spectroscopy (EDS, X-Max^N, Oxford Instruments, UK) was performed to analyze the composition of the nanoparticles. To investigate the structure of the samples, Fourier transform infrared spectroscopy (FTIR, IRAffinity-1S, SHIMADZU, Japan) was used in attenuated total reflection, and X-ray diffraction analysis (XRD, MiniFlex 600, Rigaku, Japan) was conducted in a 2θ range of 10–60 °. The zeta potential values were detected by Zetasizer nano ZS (Malvern Instruments, UK) and the hydrodynamic size and polydispersity index (PDI) of the samples were characterized by dynamic light scattering (DLS) instrument (Zetasizer nano ZS,

Malvern Instruments, UK).

2.3. *In vitro* bioactivity

The assessment of *in vitro* bioactivity (surface reactivity) of the nanoparticles was carried out in simulated body fluid (SBF) in terms of the formation of hydroxyapatite (HA) as proposed by Kokubo et al. [22]. In brief, 4 groups of BG nanoparticles (DMSNs, DMBGNs, 1Ce-DMBGNs and 3Ce-DMBGNs) were incubated in SBF at a concentration of 1 mg/mL in an orbital shaker at a constant speed of 90 rpm and temperature of 37 ◦C for up to 7 days. At each predetermined time point, the particles were collected and rinsed with DI water before being dried at 60 ◦C in an electric oven overnight. The formation of HA was evaluated by FTIR, XRD, and SEM-EDS analyses.

2.4. Propolis loading and *in vitro* release

To prepare the propolis loaded nanoparticles, propolis (20 v%, Allura Naturheilmittel GmbH, Germany) solution was firstly diluted to the concentration of 10 v% using ethanol for drug loading. Then 500 mg of each sample (DMSNs, DMBGNs and 1Ce-DMBGNs) were soaked into 10 mL of 10 v% propolis solution under stirring at room temperature in the dark for 8 h. Subsequently, the mixture was centrifuged and washed to remove non-adsorbed propolis prior to drying. The propolis loaded nanoparticles were designated as DMSNs@Pr, DMBGNs@Pr and Ce-DMBGNs@Pr, respectively. FITR analysis was performed on propolis loaded samples. The formula used for calculating the loading efficiency was:

Loading efficiency (%) = $\frac{A-B}{A}$ × 100 %

where *A* and *B* represent the initial and final concentrations of propolis, respectively.

The *in vitro* release profile of propolis was determined by immersing DMSNs@Pr, DMBGNs@Pr and Ce-DMBGNs@Pr into 10 mL of phosphate buffer saline (PBS, pH 7.4) at a concentration of 1 mg/mL in an incubator at 90 rpm shaking speed and 37 ◦C. At pre-set time points (1, 2, 4, 8, 24, 48, 72, 120, 168, 240 and 336 h), 2 mL of supernatant was extracted for measurement and 2 mL of fresh PBS was replenished. The extracted supernatant was evaluated by UV-vis spectrometer (Specord40, Analytic Jena) coupled with WinASPECT 2.5.8.0 software at a wavelength of 300 nm [23].

2.5. Statistical analysis

Each experiment was carried out at least in triplicate. The results were reported as mean values ± standard deviation (S.D.).

3. Results and discussion

The structural and morphological characteristics of materials have a profound influence on their physical and chemical properties. The morphologies and compositions of various DMBGNs were examined by TEM and SEM coupled with EDS analysis. Figure 1 shows representative TEM (left column) and SEM (middle column) images of DMSNs, DMBGNs, 1Ce-DMBGNs, 3Ce-DMBGNs and 5Ce-DMBGNs. From TEM images, center-radial dendritic shapes and opening cone-like mesopores are distinctly observed for all particles, and the particles sizes are evenly ~100 nm. Additionally, SEM results reveal that all particles show fairly homogenous spherical

shape with visibly three-dimensional mesopores and wrinkles on the surface, agreeing well with that of particles synthesized using similar approaches reported in the literature [7], [24]. Incorporation of Ca and Ce did not affect the morphologies of the particles significantly. DMBGNs, 1Ce-DMBGNs, 3Ce-DMBGNs and 5Ce-DMBGNs retain a similar size and the structure of DMSNs. Figure 1(c, f, i, l, o) show the EDS spectra of the 5 groups of particles, revealing the presence of Si, Ca, and Ce elements in the corresponding nanoparticles. Ca peaks can be found in the EDS spectrum of DMBGNs (Figure 1f). Meanwhile, both Ca and Ce peaks can be observed in the EDS spectra of 1Ce-DMBG (Figure 1i), 3Ce-DMBG (Figure 1l) and 5Ce-DMBG (Figure 1o), indicating the successful incorporation of Ca and Ce into Ce-DMBGNs.

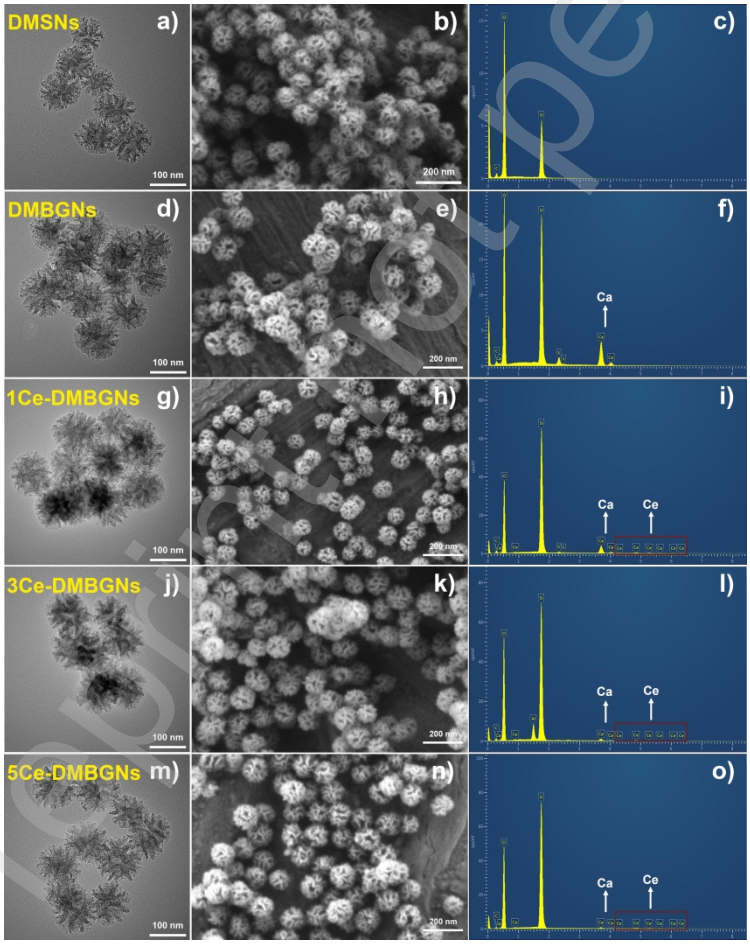

Figure 1 TEM (left), SEM images (middle) and EDS spectra (right) of DMSNs (a-c),

DMBGNs (d-f), 1Ce-DMBGNs (g-i), 3Ce-DMBGNs (j-l) and 5Ce-DMBGNs (m-o).

Table 1 Actual compositions of nanoparticles (in mol%) calculated from EDS results.

Designation	SiO_2	CaO	CeO_2
DMSNs	100	-	-
DMBGNs	85 ± 9	15 ± 9	-
1Ce-DMBGNs	89.3 ± 0.2	9.7 ± 0.2	1.0 ± 0.1
3Ce-DMBGNs	95.7 ± 0.8	3.1 ± 0.7	1.2 ± 0.1
5Ce-DMBGNs	97.6 ± 0.4	1.3 ± 0.2	1.0 ± 0.1

The actual compositions of the nanoparticles are summarized in Table 1. For DMBGNs, the calculated composition was ~85SiO_2-15CaO (mol%) determined by EDS analysis. After post-modification with different concentrations of cerium precursor, the actual compositions of these particles varied accordingly from ~85SiO_2-15CaO (mol%) for DMBGNs to ~89SiO_2-10CaO-1CeO_2 (mol%) for 1Ce-DMBGNs, ~96SiO_2-3CaO-1CeO_2 (mol%) for 3Ce-DMBGNs, and ~98SiO_2-1CaO-1CeO_2 (mol%) for 5Ce-DMBGNs. With the increasing amount of added Ce precursors in the reaction system, the actual concentrations of Ca ions in particles decreased, while Ce concentrations remained approximately constant at 1 mol%. It could be deduced that 1 mol% CeO_2 could have reached the maximum amount of Ce ions adsorbed by this type of nanoparticles. Depending on the synthesizing process, DMBGNs without heating treatment were used for Ce incorporation, as a result, most Ca ions were only

adsorbed onto the surface of silica nanoparticles, not diffusing into and entering the silicate framework [25], [26]. Moreover, during the reaction, the presence of positively charged Ca and Ce ions could adversely affect the adsorption due to the repulsion interactions, leading to reduced metallic ions adsorption onto silica nanoparticles [27]. Therefore, with higher concentration of Ce precursor solution, a greater loss of Ca ions occurred, leading to lower percentages of CaO in Ce-DMBGNs.

Table 2 Characterization results of zeta-potential, hydrodynamic size and polydispersity index values in DI water.

Designation	Zeta potential (mV)	Hydrodynamic size (nm)	PDI
DMSNs	-39 ± 5	215.4 ± 0.6	0.140
DMBGNs	-18 ± 5	221 ± 1	0.338
1Ce-DMBGNs	-32 ± 8	215 ± 1	0.306
3Ce-DMBGNs	-35 ± 7	186 ± 3	0.213
5Ce-DMBGNs	-35 ± 7	191 ± 3	0.233

The zeta potential values (Table 2) of DMSNs, DMBGNs, 1Ce-DMBGNs, 3Ce-DMBGNs and 5Ce-DMBGNs were -39 ± 5, -18 ± 5, -32 ± 8, -35 ± 7 and -35 ± 7 mV, respectively, which suggest that all nanoparticles were negatively charged due to the presence of deprotonated silanol groups. The high values of zeta potential also indicate the good stability of these nanoparticles in DI water. The zeta potential value of DMBGNs (-18 mV) was lower compared to that of DMSNs (-39 mV), probably owing to the incorporation of positive charged Ca ions. After doping with Ce ions, the zeta

potential values of nanoparticles (1Ce-DMBGNs, 3Ce-DMBGNs and 5Ce-DMBGNs) decreased to ~-30 mV, which could be attributed to the reduction of total cation percentage, as shown in EDS results. DLS measurements showed the hydrodynamic sizes of all nanoparticles were ~200 nm. In addition, the PDI values were < 0.5, indicating the homogeneous dispersion and stability of all nanoparticles in an aqueous solution [28]. After the incorporation of Ca and Ce, the PDI values increased from 0.140 for DMSNs to 0.338 for DMBGNs, 0.306 for 1Ce-DMBGNs, 0.213 for 3Ce-DMBGNs, and 0.233 for 5Ce-DMBGNs, revealing a slight decline in the dispersion of the nanoparticles.

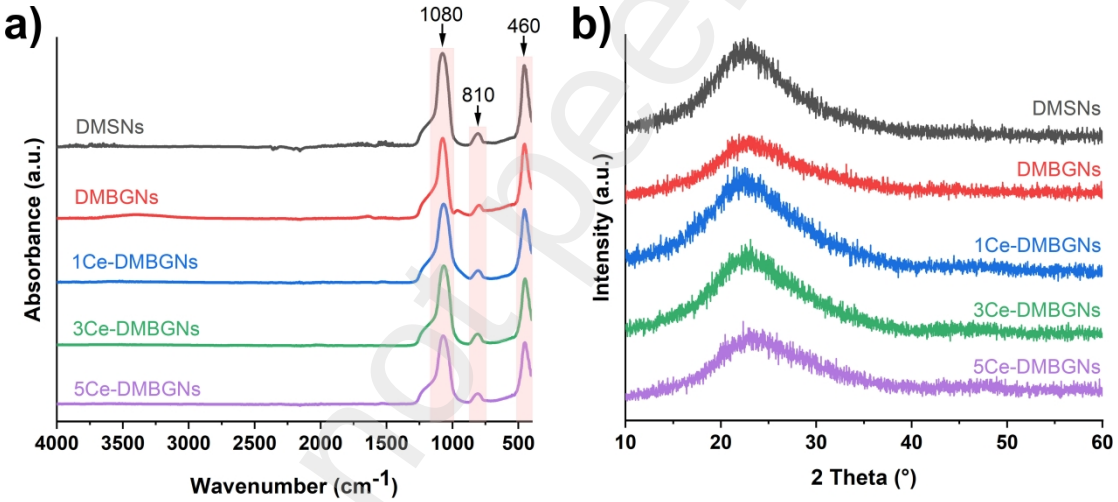

Figure 2 (a) FTIR spectra and (b) XRD patterns of DMSNs, DMBGNs, 1Ce-DMBGNs, 3Ce-DMBGNs and 5Ce-DMBGNs.

Figure 2a exhibits FTIR spectra of DMSNs, DMBGNs, 1Ce-DMBGNs, 3Ce-DMBGNs and 5Ce-DMBGNs. No significant differences can be observed among the 5 groups of nanoparticles showing typical FTIR bands of silicate BGs. The bands located at ~460 and ~810 cm^{-1} could be assigned to Si-O-Si rocking and symmetric stretching

vibrations, respectively [29]. The bands at ~1080 cm^{-1} could be attributed to the asymmetric stretching vibration of Si-O-Si bonds [30]. The presence of these components indicated the formation of a silicate network. As seen in Figure 2b, a broad band located at 2θ = ~24° corresponding to an amorphous silicate phase could be observed in XRD patterns of all nanoparticles, revealing the amorphous characteristics of Ce-DMBGNs without formation of crystalline cerium oxide nanoparticles.

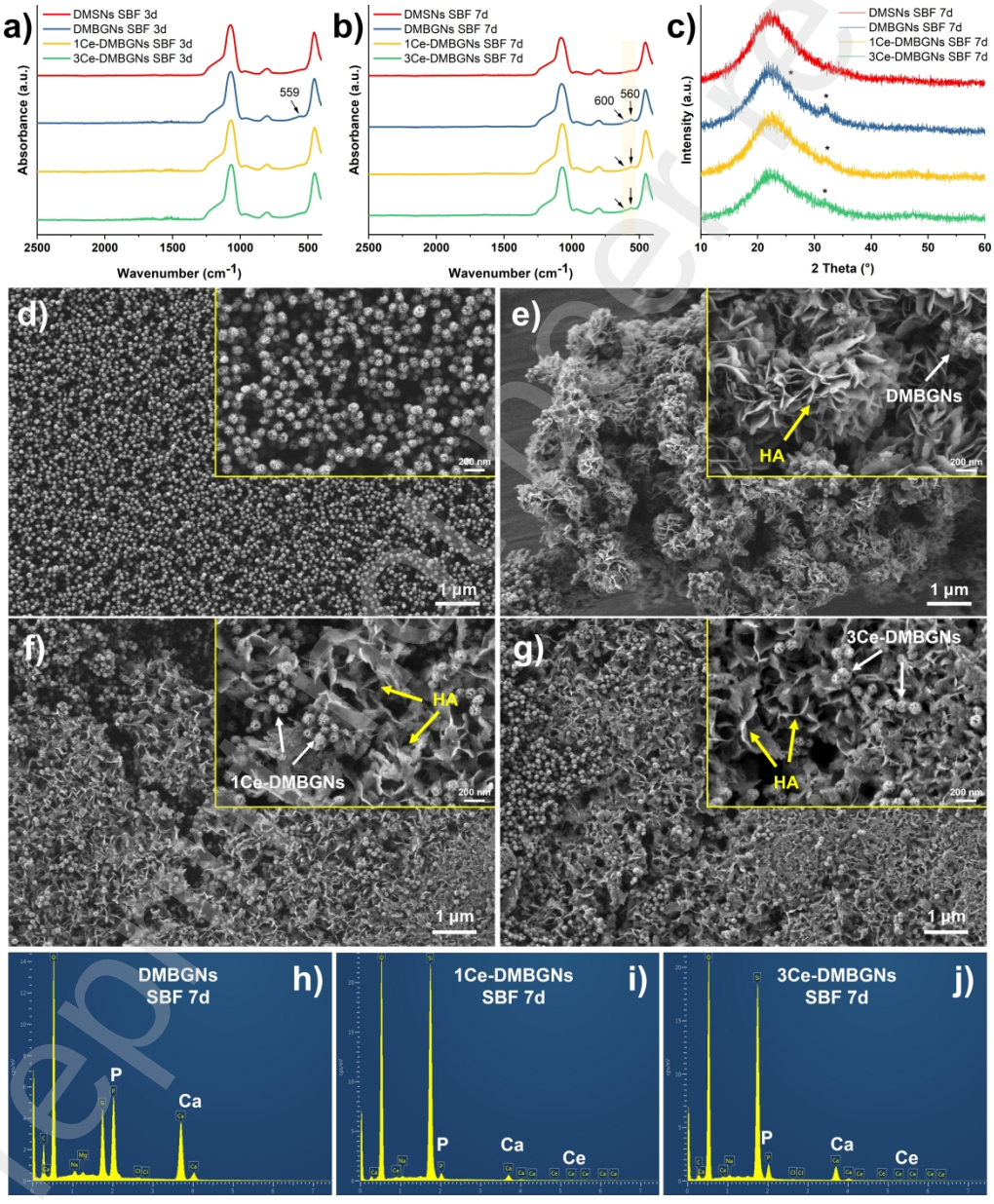

Figure 3 (a-b) FTIR spectra and (c) XRD patterns of nanoparticles after soaking in

SBF for 3 and 7 days; (d-g) SEM images at different magnifications and (h-j) EDS spectra of (d) DMSNs, (e, h) DMBGNs, (f, i) 1Ce-DMBGNs and (g, j) 3Ce-DMBGNs after soaking in SBF for 7 days.

The *in vitro* HA formation capability of nanoparticles was verified by immersing nanoparticles in SBF for 3 and 7 days. Considering the relatively low CaO content of 5Ce-DMBG, the bioactivity study was only carried out on DMBGNs, 1Ce-DMBGNs and 3Ce-DMBGNs. After soaking in SBF for 3 days, the characteristic P–O vibrational peak at ~559 cm^{-1} was only found in the FTIR spectrum of DMBGNs (Figure 3a), indicating the presence of a CaP-rich layer on the DMBGNs surfaces [31]. However, two split bands located at around 560 cm^{-1} and 600 cm^{-1} are observed in the FTIR spectra (Figure 3b) of DMBGNs, 1Ce-DMBGNs and 3Ce-DMBGNs after immersion in SBF for 7 days, which correspond to the P-O bonds of crystalline calcium phosphate phases [31], [32]. XRD patterns (Figure 3c) further confirmed the *in vitro* mineralization of the synthesized nanoparticles after soaking in SBF for 7 days. Two distinct diffraction peaks are observed at $2\theta = 25.8°$ and 32.0° on the XRD patterns of DMBG after 7 days, which can be related to hexagonal HA crystalline (JCPDS 09-0432). Additionally, diffraction peaks at approximately $2\theta = 32°$, corresponding to the lattice plane (112) of HA, are observed in the XRD diffraction patterns of 1Ce-DMBGNs and 3Ce-DMBGNs after incubating in SBF for 7 days. The formation of a HA phase was further supported by SEM investigation. After immersion in SBF for 7 days, petal-like and needle-like crystals were clearly observed on DMBGNs, 1Ce-DMBGNs and 3Ce-DMBGNs, except

for DMSNs, revealing the crystalline HA formation on these nanoparticles. To verify the composition of the formed crystals, EDS analysis was conducted on DMBGNs, 1Ce-DMBGNs and 3Ce-DMBGNs. The EDS spectra confirmed the existence of P and Ca elements, indicating the formation of Ca-P species. The Ca/P molar ratios were 1.61 for DMBG, 1.50 for 1Ce-DMBG, 1.53 for 3Ce-DMBG, respectively, which means that the formed HA crystalline phase was Ca-deficient and the Ca/P molar ratio could increase with soaking time [33].

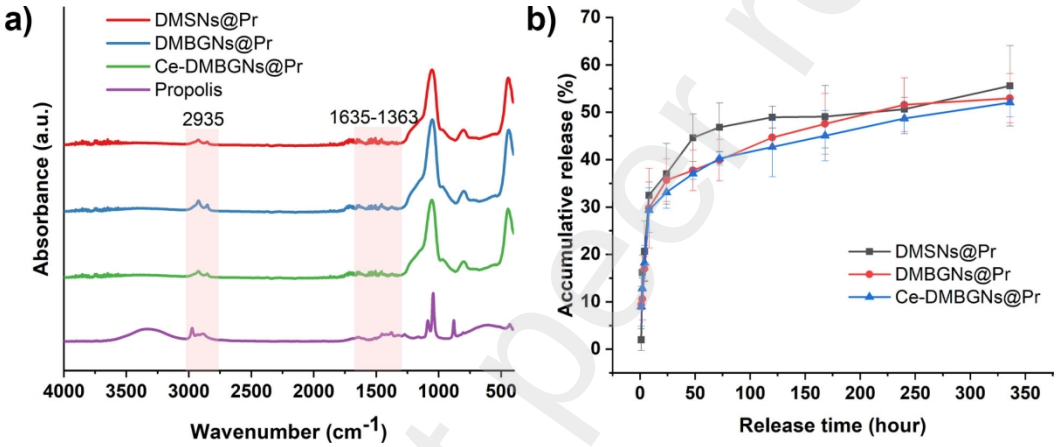

Figure 4 (a) FTIR spectra of propolis and propolis loaded nanoparticles (DMSNs@Pr, DMBGNs@Pr and Ce-DMBGNs@Pr); (b) propolis release profiles of DMSNs@Pr, DMBGNs@Pr and Ce-DMBGNs@Pr.

Propolis is a naturally active product including flavonoids, diterpenic acids, phenolic acids, amino acids, etc. [34]. DMBGNs and Ce-DMBGNs can be efficiently loaded with propolis with a loading efficiency of 66.1 ± 6.1 % and 65.9 ± 6.3 %, respectively, which however were lower than that of DMSNs (71.6 ± 3.8 %). This reduction in loading efficiency is probably due to the decreased specific surface area after post modification [7], [35]. FTIR analysis was done to investigate the presence of propolis in the

nanoparticles. As seen in the FITR spectra of DMSNs@Pr, DMBGNs@Pr and Ce-DMBGNs@Pr, bands located at ~2935 cm^{-1} could be attributed to ketone and phenol groups in propolis [36]. In addition, bands located in the range of 1363-1635 cm^{-1} could be assigned to stretching vibrations of C=O and C-O groups of flavonoids, bending vibrations of N-H groups of amino acid [23], [36], confirming the successful loading of propolis into nanoparticles. Figure 4b shows accumulative release profiles of propolis from DMSNs@Pr, DMBGNs@Pr and Ce-DMBGNs@Pr. A burst release occurring within initial 8 h reaching ~32, ~30, ~29 % for DMSNs@Pr, DMBGNs@Pr and Ce-DMBGNs@Pr, respectively, was observed, which is likely due to the portion of propolis deposited on the surface of the particles. Afterwards, compared to DMSNs@Pr, more slightly sustained and slower release was achieved for DMBGNs@Pr and especially for Ce-DMBG@Pr, and finally up to concentrations of ~56 % for DMSNs@Pr, ~53 % for DMBGNs@Pr and ~52 % for Ce-DMBGNs@Pr. The possible reason is the blocking of the mesopores during the release process by water-insoluble components in propolis, e.g., resin and wax. In conclusion, all three groups of nanoparticles revealed sustained release behavior of propolis. Ce-DMBGNs especially have significant potential as therapeutic molecule (including propolis) carriers with sustained release capability. Being loaded with propolis, Ce-DMBGNs are expected to exert superior antibacterial and antioxidant effects for bone repair applications, particularly in the context of infection, by exploiting the synergistic effect of Ce and propolis release.

4. Conclusions

In this study, we prepared DMSNs via a sol-gel approach by using dual templates at

ultralow concentration in an organic solvent free system. By applying the impregnation strategy, Ca and Ce can be easily incorporated into silicate network resulting in nearly spherical DMBGNs and Ce-DMBGNs. Both DMBGNs and Ce-DMBGNs showed favorable apatite-forming capacity in SBF indicating their bioactivity *in vitro*. After being loaded with propolis, DMBGNs and Ce-DMBGNs exhibited sustained release behavior with low initial burst release of propolis. The results of this study thus imply that both DMBGNs and Ce-DMBGNs are promising materials for bone regeneration, local drug and ion delivery. The kinetic of Ce and Ca release remains to be investigated which should be tuned taking into account the biomolecule (propolis) release kinetics.

Acknowledgments

Zhiyan Xu would like to acknowledge the fellowship from the China Scholarship Council (CSC, No. 202006740028). Authors would also thank CITIUS, central services of the Universidad de Sevilla (Spain), for the use of scanning-transmission electron microscope instrument.

Conflict and Interest

The authors declare no conflict of interest.

References

[1] H. Zhu et al., “3D Bioprinting of Multifunctional Dynamic Nanocomposite Bioinks Incorporating Cu-Doped Mesoporous Bioactive Glass Nanoparticles for Bone Tissue Engineering,” Small, vol. 18, no. 12, p. 2104996, 2022, doi: 10.1002/smll.202104996.

[2] A. El-Fiqi, J.-H. Kim, and H.-W. Kim, “Osteoinductive Fibrous Scaffolds of

Biopolymer/Mesoporous Bioactive Glass Nanocarriers with Excellent Bioactivity and Long-Term Delivery of Osteogenic Drug," ACS Appl. Mater. Interfaces, vol. 7, no. 2, pp. 1140–1152, Jan. 2015, doi: 10.1021/am5077759.

[3] C. Wu and J. Chang, "Mesoporous bioactive glasses: structure characteristics, drug/growth factor delivery and bone regeneration application," Interface Focus, vol. 2, no. 3, pp. 292–306, Mar. 2012, doi: 10.1098/rsfs.2011.0121.

[4] I. Izquierdo-Barba and M. Vallet-Regí, "Mesoporous bioactive glasses: Relevance of their porous structure compared to that of classical bioglasses," Biomed. Glas., vol. 1, no. 1, Nov. 2015, doi: 10.1515/bglass-2015-0014.

[5] C. H. Kong, C. Steffi, Z. Shi, and W. Wang, "Development of mesoporous bioactive glass nanoparticles and its use in bone tissue engineering," J. Biomed. Mater. Res. B Appl. Biomater., vol. 106, no. 8, pp. 2878–2887, 2018, doi: 10.1002/jbm.b.34143.

[6] B. Sui, X. Liu, and J. Sun, "Dual-Functional Dendritic Mesoporous Bioactive Glass Nanospheres for Calcium Influx-Mediated Specific Tumor Suppression and Controlled Drug Delivery in Vivo," ACS Appl. Mater. Interfaces, vol. 10, no. 28, pp. 23548–23559, Jul. 2018, doi: 10.1021/acsami.8b05616.

[7] X. Han, A. Erkan, Z. Xu, Y. Chen, A. R. Boccaccini, and K. Zheng, "Organic solvent-free synthesis of dendritic mesoporous bioactive glass nanoparticles with remineralization capability," Mater. Lett., vol. 320, p. 132366, Aug. 2022, doi: 10.1016/j.matlet.2022.132366.

[8] K. Zheng, B. Sui, K. Ilyas, and A. R. Boccaccini, "Porous bioactive glass micro- and nanospheres with controlled morphology: developments, properties and emerging

biomedical applications," Mater. Horiz., vol. 8, no. 2, pp. 300–335, Feb. 2021, doi: 10.1039/D0MH01498B.

[9] C. Xu, C. Lei, Y. Wang, and C. Yu, "Dendritic Mesoporous Nanoparticles: Structure, Synthesis and Properties," Angew. Chem., vol. 134, no. 12, p. e202112752, 2022, doi: 10.1002/ange.202112752.

[10] Y. Wang, X. Du, Z. Liu, S. Shi, and H. Lv, "Dendritic fibrous nano-particles (DFNPs): rising stars of mesoporous materials," J. Mater. Chem. A, vol. 7, no. 10, pp. 5111–5152, Mar. 2019, doi: 10.1039/C8TA09815H.

[11] K. Zheng and A. R. Boccaccini, "Sol-gel processing of bioactive glass nanoparticles: A review," Adv. Colloid Interface Sci., vol. 249, pp. 363–373, Nov. 2017, doi: 10.1016/j.cis.2017.03.008.

[12] H. Zhu, K. Zheng, and A. R. Boccaccini, "Multi-functional silica-based mesoporous materials for simultaneous delivery of biologically active ions and therapeutic biomolecules," Acta Biomater., vol. 129, pp. 1–17, Jul. 2021, doi: 10.1016/j.actbio.2021.05.007.

[13] C. Wu et al., "Copper-containing mesoporous bioactive glass scaffolds with multifunctional properties of angiogenesis capacity, osteostimulation and antibacterial activity," Biomaterials, vol. 34, no. 2, pp. 422–433, Jan. 2013, doi: 10.1016/j.biomaterials.2012.09.066.

[14] F. Kurtuldu et al., "Cerium and gallium containing mesoporous bioactive glass nanoparticles for bone regeneration: Bioactivity, biocompatibility and antibacterial activity," Mater. Sci. Eng. C, vol. 124, p. 112050, May 2021, doi:

10.1016/j.msec.2021.112050.

[15] G. Lusvardi, F. Fraulini, S. D'Addato, and A. Zambon, "Loading with Biomolecules Modulates the Antioxidant Activity of Cerium-Doped Bioactive Glasses," ACS Biomater. Sci. Eng., vol. 8, no. 7, pp. 2890–2898, Jul. 2022, doi: 10.1021/acsbiomaterials.2c00283.

[16] A. Zambon, G. Malavasi, A. Pallini, F. Fraulini, and G. Lusvardi, "Cerium Containing Bioactive Glasses: A Review," ACS Biomater. Sci. Eng., vol. 7, no. 9, pp. 4388–4401, Sep. 2021, doi: 10.1021/acsbiomaterials.1c00414.

[17] A. El-Fiqi, R. Allam, and H.-W. Kim, "Antioxidant cerium ions-containing mesoporous bioactive glass ultrasmall nanoparticles: Structural, physico-chemical, catalase-mimic and biological properties," Colloids Surf. B Biointerfaces, vol. 206, p. 111932, Oct. 2021, doi: 10.1016/j.colsurfb.2021.111932.

[18] Z. Khurshid, M. Naseem, M. S. Zafar, S. Najeeb, and S. Zohaib, "Propolis: A natural biomaterial for dental and oral healthcare," J. Dent. Res. Dent. Clin. Dent. Prospects, vol. 11, no. 4, pp. 265–274, 2017, doi: 10.15171/joddd.2017.046.

[19] V. R. Pasupuleti, L. Sammugam, N. Ramesh, and S. H. Gan, "Honey, Propolis, and Royal Jelly: A Comprehensive Review of Their Biological Actions and Health Benefits," Oxid. Med. Cell. Longev., vol. 2017, p. e1259510, Jul. 2017, doi: 10.1155/2017/1259510.

[20] A. M. Gómez-Caravaca, M. Gómez-Romero, D. Arráez-Román, A. Segura-Carretero, and A. Fernández-Gutiérrez, "Advances in the analysis of phenolic compounds in products derived from bees," J. Pharm. Biomed. Anal., vol. 41, no. 4,

pp. 1220–1234, Jun. 2006, doi: 10.1016/j.jpba.2006.03.002.

[21] K. Schuhladen, J. A. Roether, and A. R. Boccaccini, “Bioactive glasses meet phytotherapeutics: The potential of natural herbal medicines to extend the functionality of bioactive glasses,” Biomaterials, vol. 217, p. 119288, Oct. 2019, doi: 10.1016/j.biomaterials.2019.119288.

[22] T. Kokubo and H. Takadama, “How useful is SBF in predicting in vivo bone bioactivity?,” Biomaterials, vol. 27, no. 15, pp. 2907–2915, May 2006, doi: 10.1016/j.biomaterials.2006.01.017.

[23] R. Bilginer, D. Ozkendir-Inanc, U. H. Yildiz, and A. Arslan-Yildiz, “Biocomposite scaffolds for 3D cell culture: Propolis enriched polyvinyl alcohol nanofibers favoring cell adhesion,” J. Appl. Polym. Sci., vol. 138, no. 17, p. 50287, 2021, doi: 10.1002/app.50287.

[24] P. C. Liu et al., “A dual-templating strategy for the scale-up synthesis of dendritic mesoporous silica nanospheres,” Green Chem., vol. 19, no. 23, pp. 5575–5581, 2017, doi: 10.1039/c7gc02139a.

[25] S. Lin, C. Ionescu, K. J. Pike, M. E. Smith, and J. R. Jones, “Nanostructure evolution and calcium distribution in sol–gel derived bioactive glass,” J. Mater. Chem., vol. 19, no. 9, pp. 1276–1282, 2009, doi: 10.1039/B814292K.

[26] M. Kapp, C. Li, Z. Xu, A. R. Boccaccini, and K. Zheng, “Protein Adsorption on SiO2-CaO Bioactive Glass Nanoparticles with Controllable Ca Content,” Nanomaterials, vol. 11, no. 3, Art. no. 3, Mar. 2021, doi: 10.3390/nano11030561.

[27] K. Zheng, X. Dai, M. Lu, N. Hüser, N. Taccardi, and Aldo. R. Boccaccini,

"Synthesis of copper-containing bioactive glass nanoparticles using a modified Stöber method for biomedical applications," Colloids Surf. B Biointerfaces, vol. 150, pp. 159–167, Feb. 2017, doi: 10.1016/j.colsurfb.2016.11.016.

[28] X. Liu, B. Sui, and J. Sun, "Size- and shape-dependent effects of titanium dioxide nanoparticles on the permeabilization of the blood–brain barrier," J. Mater. Chem. B, vol. 5, no. 48, pp. 9558–9570, Dec. 2017, doi: 10.1039/C7TB01314K.

[29] K. Zheng et al., "Timing of calcium nitrate addition affects morphology, dispersity and composition of bioactive glass nanoparticles," RSC Adv., vol. 6, no. 97, pp. 95101–95111, 2016, doi: 10.1039/C6RA05548F.

[30] K. Zheng et al., "Ag modified mesoporous bioactive glass nanoparticles for enhanced antibacterial activity in 3D infected skin model," Mater. Sci. Eng. C, vol. 103, p. 109764, Oct. 2019, doi: 10.1016/j.msec.2019.109764.

[31] X. Yan et al., "The in-vitro bioactivity of mesoporous bioactive glasses," Biomaterials, vol. 27, no. 18, pp. 3396–3403, Jun. 2006, doi: 10.1016/j.biomaterials.2006.01.043.

[32] D. C. Clupper, J. J. Mecholsky, G. P. LaTorre, and D. C. Greenspan, "Bioactivity of tape cast and sintered bioactive glass-ceramic in simulated body fluid," Biomaterials, vol. 23, no. 12, pp. 2599–2606, Jun. 2002, doi: 10.1016/S0142-9612(01)00398-2.

[33] A. Bari et al., "Copper-containing mesoporous bioactive glass nanoparticles as multifunctional agent for bone regeneration," Acta Biomater., vol. 55, pp. 493–504, Jun. 2017, doi: 10.1016/j.actbio.2017.04.012.

[34] M. Stojko, D. Wolny, and J. Włodarczyk, "Nonwoven Releasing Propolis as a

Potential New Wound Healing Method—A Review," Molecules, vol. 26, no. 18, Art. no. 18, Jan. 2021, doi: 10.3390/molecules26185701.

[35] K. Zheng et al., "Antioxidant mesoporous Ce-doped bioactive glass nanoparticles with anti-inflammatory and pro-osteogenic activities," Mater. Today Bio, vol. 5, p. 100041, Jan. 2020, doi: 10.1016/j.mtbio.2020.100041.

[36] M. Ahmed, M. Amirat, S. Aissat, M. A. Aissa, and B. Khiati, "FTIR characterization of Sahara honey and propolis and evaluation of its anticandidal potentials," Acta Sci. Nat., vol. 7, no. 3, pp. 46–57, Nov. 2020, doi: 10.2478/asn-2020-0032.